

# IMPROVED STRAPDOWN INERTIAL MEASUREMENT UNIT CALIBRATION PROCEDURES

Paul G. Savage  
Strapdown Associates, Inc.

WBN-14028  
www.strapdownassociates.com  
June 2, 2020

Originally presented at the 2018 IEEE/ION Position, Location and Navigation  
Symposium (PLANS), Monterey, CA, USA, 23-26 April, 2018  
Published by the IEEE, DOI: 10.1109/PLANS.2018.8373422

## ABSTRACT

This article describes an improved strapdown rotation test (SRT) for calibrating the compensation coefficients in a strapdown inertial measurement unit (IMU). The SRT consists of a set of IMU rotation sequences and processing routines that enable precision determination of IMU gyro/accelerometer misalignment, gyro/accelerometer scale factor, and accelerometer bias calibration errors, all without requiring precision rotation fixtures and IMU mounting procedures. A key advantage for the new procedure is the ability to measure an individual sensor error using a single rotation sequence (as opposed to multiple rotation sequences required with previous approaches). The improved SRT is compatible with a broad range of IMU types from aircraft accuracy inertial navigation systems to low cost micro-machined electronic module systems (MEMS). This article describes the general theory for the improved rotation tests, rotation test operations, data collection during test, post-test data processing, rotation test fixture requirements, and an analysis of SRT accuracy in determining IMU sensor errors.

## 1. INTRODUCTION

The Strapdown Rotation Test (SRT) is a test procedure designed for rapid measurement/calibration of inertial sensor error parameters in a strapdown inertial measurement unit (IMU). The principle advantage of the SRT is the ability to precisely determine sensor errors (e.g., misalignments) to  $\mu\text{rad}$  accuracy using moderate accuracy (one milli-rad) rotation test fixturing. The SRT is performed by executing a series of IMU rotation sequences with the IMU mounted on a two-axis rotation fixture.

In the original SRT concept disclosed in 1977 [1], recorded test measurements were the rate of change of inertially computed horizontal velocity following each rotation sequence. Horizontal velocity was calculated within the IMU using standard strapdown inertial navigation software routines. Before initiating inertial navigation, each rotation sequence was preceded by a stationary inertial-sensor-based alignment of IMU computed attitude.

The basic principle underlying the [1] approach is that following initial alignment, an IMU with ideal (error free) inertial sensors will have zero computed inertial velocity when stationary

following a rotation sequence. Non-zero stationary velocity rates measure the effect of sensor errors excited by the rotation sequence. In general, a stationary inertial alignment will produce zero computed horizontal velocity rate at inertial navigation entry [2, Sect. 14.5]. Following inertial alignment, an SRT rotation sequence will then excite gyro errors into inertial navigation computed attitude and reposition the accelerometers (and their errors), both effects generating non-zero horizontal inertial velocity rate when stationary at rotation sequence completion. Stationary horizontal velocity rate following a rotation sequence then became the primary [1] measure of composite gyro/accelerometer error effects, each rotation sequence producing a different combination of sensor errors on the measurement. Analytical routines within the SRT translated the measurements into the sensor errors that created them (an analytical linear inversion process).

Ref. [3] replaced the inertial alignment preceding each rotation sequence by a single inertial alignment at SRT start. Inertial navigation velocity rate was then recorded at stationary periods between rotation sequences. Measurements for sensor error determination were the difference in stationary horizontal velocity rates before and after each rotation sequence. As in [1], individual sensor errors were determined by processing the group of measurements at SRT completion.

The [3] single alignment approach with before/after rotation sequence measurement was then incorporated into a revised [1] concept [2, Sect. 18.4] that also replaced the [1, 3] velocity rate measurements with averaged horizontal accelerations from a strapdown “analytic platform”. An analytic platform is a computational element in a strapdown IMU that incorporates a direction cosine matrix (DCM) to rotate (“transform”) rotating strapdown accelerometer signals into a non-rotating reference coordinate frame. The resulting non-rotating accelerations emulate what would be output from accelerometers directly mounted on a physically controlled non-rotating gyro-stabilized gimballed platform. For the SRT, the analytic platform would reside as software in the IMU under test or in the SRT test computer. The latter concept is depicted in Fig. 1, the DCM being calculated in the “Attitude Computation” block using IMU gyro measured inertial rotation rates corrected for earth’s inertial rotation rate.

This article is a condensed version of the three part [4, 5, 6] article describing the latest form of the SRT. The new SRT eliminates the [1, 2, 3] inertial sensor-based DCM alignment prior to executing rotation sequences, thereby expanding applicability to IMUs with sensors lacking the accuracy required for inertial alignment, e.g., MEMS (micro-machined electronic system) IMUs. Each rotation sequence in the new SRT has been designed for independent measurement and determination of a particular sensor error parameter, thus, simplifying measurement data processing, reducing second order error buildup in attitude and potential sensor error shifts over the time required to determine a sensor error (compared with [1, 2, 3] where the time to determine a sensor error spanned inertial DCM alignment and multiple rotation sequence measurements), and reducing sensor error parameter determination uncertainty caused in [1, 2, 3] by inverting multiple measurements, each having modeling approximation errors. The underlying SRT principle, however, remains the same; that the change in stationary horizontal acceleration over a rotation sequence is a measure of IMU sensor calibration errors.

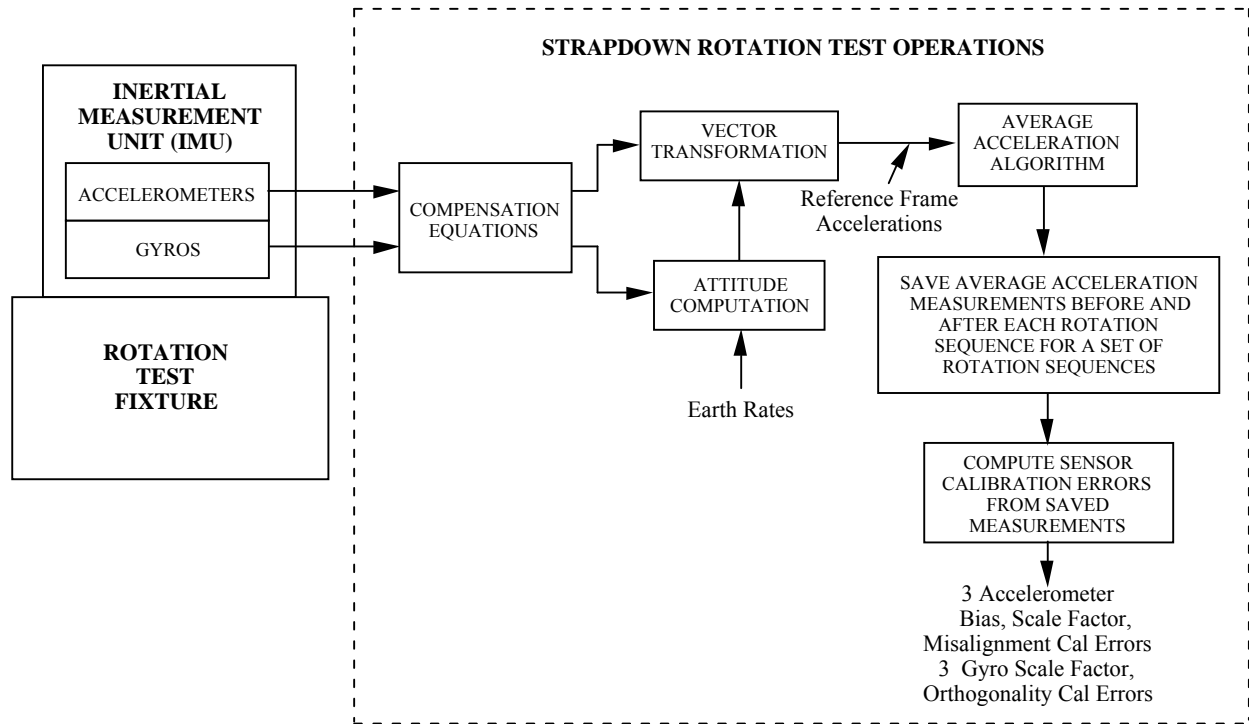


Fig. 1. Strapdown Rotation Test (SRT) Setup

This article describes the improved SRT and how it would be implemented using a modest accuracy (e.g., 0.1 deg) two-axis rotation test fixture. Section 2 defines notation, coordinate frames, and parameter definitions used in the article. Sections 3 – 7 define the improved SRT rotation sequences, data processing routines for generating SRT acceleration measurements, and computational routines for extracting sensor calibration errors from the measurements. Section 8 describes a modern day iteration process that can be used for SRT accuracy enhancement. Section 9 provides a detailed error analysis showing how SRT sensor error determination accuracy is impacted by IMU mounting error on the rotation test fixture, rotation fixture error in executing SRT rotations, uncertainty in rotation fixture orientation relative to north/down, approximations in SRT processing equations, and IMU sensor calibration errors prior to SRT execution. Section 10 describes how outputs from an IMU with SRT recalibrated sensors can then be used to determine IMU sensor assembly to mount misalignments for calibration correction.

## 2. NOTATION, COORDINATE FRAMES, AND PARAMETER DEFINITIONS

### 2.1 NOTATION

$\underline{V}$  = Vector having length and direction.

$\underline{V}^A$  = Column matrix with elements equal to projections of  $\underline{V}$  on coordinate frame  $A$  axes, i.e., the dot product of  $\underline{V}$  with a unit vector parallel to each coordinate axis.

$(\underline{V}^A \times)$  = Skew symmetric (or cross-product) square matrix form of  $\underline{V}^A$  represented by

$$\begin{bmatrix} 0 & -V_{ZA} & V_{YA} \\ V_{ZA} & 0 & -V_{XA} \\ -V_{YA} & V_{XA} & 0 \end{bmatrix}$$

where  $-V_{XA}$ ,  $V_{YA}$ ,  $V_{ZA}$  are components of  $\underline{V}^A$ . The matrix product of  $(\underline{V}^A \times)$  with another  $A$  frame projected vector equals the cross-product of  $\underline{V}^A$  with the vector, i.e.,  $(\underline{V}^A \times) \underline{W}^A = \underline{V}^A \times \underline{W}^A$ .

$C_{A2}^{A1}$  = Frame  $A_2$  to  $A_1$  direction cosine matrix (DCM) that transforms a vector from its  $A_2$  projection to its  $A_1$  projection, i.e.,  $\underline{V}^{A1} = C_{A2}^{A1} \underline{V}^{A2}$ . An important property of  $C_{A2}^{A1}$  is that its inverse equals its transpose.

$\dot{()}$  = Derivative  $\frac{d()}{dt}$  of parameter  $()$  with respect to time  $t$ .

## 2.2 COORDINATE FRAMES

$B$  = Sensor frame fixed relative to IMU inertial sensor axes that rotates with the IMU. The  $B$  frame angular orientation relative to sensor axes is arbitrary based on user preferences.

$B_{Strt}$  = Non-rotating coordinate frame relative to the earth and aligned with the  $B$  frame at the start of an SRT rotation sequence. Nominally, one of the  $B_{Strt}$  axes would be aligned with the local vertical if the IMU being tested is perfectly mounted on an idealized rotation fixture.

$B_{End}$  = Non-rotating coordinate frame relative to the earth and aligned with  $B$  at the end of a rotation sequence.

$B_{i,Strt}$  = Non-rotating coordinate frame relative to the earth and aligned with  $B$  at the start of rotation  $i$  in a rotation sequence.

$B_{i,End}$  = Non-rotating coordinate frame relative to the earth and aligned with  $B$  at the end of rotation  $i$  in a rotation sequence.

$MARS$  = Designation for a “mean-angular-rate-sensor”  $B$  frame selection, the orthogonal frame that best fits around the actual strapdown gyro input axes.

$NED$  = Earth fixed coordinate frame with axes aligned to local north, east, down directions.

## 2.3 PARAMETER DEFINITIONS

$\underline{\alpha}^B$  = Angular error vector in  $B$  frame coordinates between the nominal and actual  $B$  frames caused by IMU mounting error on the rotation fixture, rotation fixture installation error, and rotation execution error.

$\underline{\alpha}_{Strt}^B, \underline{\alpha}_{End}^B = \underline{\alpha}^B$  at rotation sequence start and end.

$\underline{a}_{SF}^B$  = True specific force acceleration vector in  $B$  frame coordinates.

$\tilde{\underline{a}}_{SF}^B$  = IMU accelerometer measurements of  $\underline{a}_{SF}^B$ .

$\hat{\underline{a}}_{SF}^{BStrt}$  =  $\tilde{\underline{a}}_{SF}^B$  transformed to the  $B_{Strt}$  frame by SRT computation.

$\left(\hat{\underline{a}}_{SF}^{BStrt}\right)_{StrtAvg}$ ,  $\left(\hat{\underline{a}}_{SF}^{BStrt}\right)_{EndAvg}$  =  $\hat{\underline{a}}_{SF}^{BStrt}$  average values when the IMU is stationary at start and end of a rotation sequence.

$\hat{\underline{a}}_{SF}^{BStrt}$ ,  $\hat{\underline{a}}_{SF}^{BEnd}$   $\equiv$   $\left(\hat{\underline{a}}_{SF}^{BStrt}\right)_{StrtAvg}$ ,  $\left(\hat{\underline{a}}_{SF}^{BStrt}\right)_{EndAvg}$ .

$\underline{a}_{SF}^{BStrt}$ ,  $\underline{a}_{SF}^{BEnd}$  = True specific force ( $\underline{a}_{SF}^B$ ) at the start and end of a rotation sequence when the IMU is stationary.

$A_{SF}^{BStrt}$ ,  $A_{SF}^{BEnd}$  = Diagonal matrices with elements of unity magnitude and sign (plus or minus) of  $\underline{a}_{SF}^{BStrt}$ ,  $\underline{a}_{SF}^{BEnd}$ . Because  $\underline{a}_{SF}^{BStrt}$ ,  $\underline{a}_{SF}^{BEnd}$  are upward, the diagonal elements of  $A_{SF}^{BStrt}$ ,  $A_{SF}^{BEnd}$  equal the negative of  $\underline{u}_{Dwn}^{BStrt}$ ,  $\underline{u}_{Dwn}^{BEnd}$ .

$\hat{\underline{a}}_{StrtDown}^{BStrt}$ ,  $\hat{\underline{a}}_{EndDown}^{BStrt}$  = SRT calculated downward IMU acceleration measurements at rotation sequence start and end.

$\hat{\underline{a}}_{Downk}^{BStrt}$ ,  $\hat{\underline{a}}_{Downk}^{BEnd}$  = Values of  $\hat{\underline{a}}_{StrtDown}^{BStrt}$  and  $\hat{\underline{a}}_{EndDown}^{BStrt}$  for rotation sequence  $k$ .

$\underline{a}_{StrtDown}^{BStrt}$ ,  $\underline{a}_{EndDown}^{BStrt}$  = SRT error model approximations for  $\hat{\underline{a}}_{StrtDown}^{BStrt}$ ,  $\hat{\underline{a}}_{EndDown}^{BStrt}$ .

$\dot{\beta}_i$  = IMU angular rate around rotation axis  $i$ .

$\hat{C}_B^{BStrt}$  = DCM computed with IMU gyro data.

$C_{Bi,Strt}^{BStrt}$ ,  $C_{BEnd}^{BStrt}$  = DCMs in measurement error models.

$\hat{C}_{NED}^{BStrt}$  = Approximated DCM based on IMU orientation.

$\delta\underline{a}_{SF}^{BStrt}$ ,  $\delta\underline{a}_{SF}^{BEnd}$  = Errors in  $\hat{\underline{a}}_{SF}^{BStrt}$  at the start and end of a rotation sequence in  $B_{Strt}$  and  $B_{End}$  coordinates.

$\delta\underline{\omega}_{Rndm}$ ,  $\delta\underline{\omega}_{Quant}$  = Gyro triad random and quantization output noise vectors.

$\delta x_k$  = Error in determining sensor error  $x_k$  due to SRT measurement approximation errors.

$\Delta\underline{\hat{a}}_H^{BStrt}$  = The difference between stationary horizontal acceleration measurements in the  $B_{Strt}$  frame at the start and end of a rotation sequence. SRT calculated as the difference between the horizontal components of  $\hat{\underline{a}}_{SF}^{BStrt}$  and  $\hat{\underline{a}}_{SF}^{BStrt}$ .

$\Delta\underline{\hat{a}}_{jk}^{BStrt}$  = Component  $j$  ( $x$ ,  $y$ , or  $z$ ) of  $\Delta\underline{\hat{a}}_H^{BStrt}$  for rotation sequence  $k$ .

$\Delta\underline{\hat{a}}_H^{BStrt}$  = SRT error model approximation for  $\Delta\underline{\hat{a}}_H^{BStrt}$ .

$\Delta a_{jk}^{BStrt}$  = Component  $j$  ( $x$ ,  $y$ , or  $z$ ) of  $\Delta \underline{a}_H^{BStrt}$  for rotation sequence  $k$ .

$e(\ )$  = SRT parameter ( ) model approximation error.

$e\left(\phi_{-End}^{BStrt}\right)_{GyroBias_{Rot}}$  = Approximation error in  $\phi_{-End}^{BStrt}$  due to neglecting gyro bias effects during a rotation sequence.

$e\left(\Delta \underline{a}_H^{BStrt}\right)_{GyroBias}$  = Approximation error in  $\Delta \underline{a}_H^{BStrt}$  due to neglected gyro bias effects in  $\phi_{-End}^{BStrt}$ .

$e\left(\Delta a_{jk}^{BStrt}\right)_{GyroBias} = e\left(\Delta \underline{a}_H^{BStrt}\right)_{GyroBias}$  component  $j$  ( $x$ ,  $y$ , or  $z$ ) for rotation sequence  $k$ .

$F_{Meas}$  = Measurement averaging filter output scale factor to constant input.

$g$  = Plumb-bob gravity magnitude at the test site.

$H_k$  = Coefficient connecting  $\Delta a_{jk}^{BStrt}$  to  $x_k$ .

$i$  = Subscript designating the rotation number in a particular SRT rotation sequence.

$I$  = Identity matrix.

$\underline{\kappa}_{Bias}$ ,  $\kappa_{LinScal}$ ,  $\kappa_{Mis}$ ,  $\kappa_{Asym}$  = Gyro triad bias error vector and linear scale factor, misalignment, asymmetrical scale factor error matrices.

$\kappa_i$ ,  $\kappa_{ii}$ ,  $\kappa_{ij}$ ,  $\kappa_{iii}$  = Gyro  $i$  components of  $\underline{\kappa}_{Bias}$ ,  $\kappa_{LinScal}$ ,  $\kappa_{Mis}$ ,  $\kappa_{Asym}$ .

$l$  = Latitude of the test site.

$\underline{\lambda}_{Bias}$ ,  $\lambda_{LinScal}$ ,  $\lambda_{Mis}$ ,  $\lambda_{Asym}$  = Accelerometer triad bias error vector and linear scale factor, misalignment, asymmetrical scale-factor error matrices.

$\lambda_i$ ,  $\lambda_{ii}$ ,  $\lambda_{ij}$ ,  $\lambda_{iii}$  = Accelerometer  $i$  components of  $\underline{\lambda}_{Bias}$ ,  $\lambda_{LinScal}$ ,  $\lambda_{Mis}$ ,  $\lambda_{Asym}$ .

$\underline{\lambda}_{RndmStrt}$ ,  $\underline{\lambda}_{RndmEnd}$ ,  $\underline{\lambda}_{QuantStrt}$ ,  $\underline{\lambda}_{QuantEnd}$  = Accelerometer triad random and quantization output noise during SRT stationary measurements at the start and end of a rotation sequence.

$\mu_{ij}$  = Accelerometer  $i$  misalignment to the *MARS B* frame axis  $j$ .

$n$  = Subscript designating rotation number  $i$  for the last rotation in a particular SRT rotation sequence.

$\omega_e$  = Magnitude of earth inertial rotation rate.

$\underline{\omega}_e^{NED}$  = Earth rotation rate vector in *NED* coordinates.

$\underline{\omega}_e^{BStrt}$ ,  $\hat{\underline{\omega}}_e^{BStrt}$  = Nominal and SRT estimated earth inertial rotation rate vectors in *BStrt* coordinates.

$\tilde{\underline{\omega}}^B$  = IMU gyro triad measurement of the inertial angular rotation rate vector in the *B* frame.

$\underline{\omega}_{EB}^B$  = *B* frame angular rate relative to the earth (*EB* subscript) in *B* frame coordinates (superscript).

$\Omega_{EBSign}^B$  = Diagonal matrix with elements of unity magnitude and sign (plus or minus) of  $\underline{\omega}_{EB}^B$ .

$\underline{\phi}^{B_{Strt}}, \underline{\phi}^{B_{End}}$  = Rotation angle error vector imbedded within  $\hat{C}_B^{B_{Strt}}$  during and at the end of a rotation sequence.

$\theta_i$  = Signed magnitude of angular rotation around axis  $i$ .

$t_{Strt}$  = Time at the start of an SRT rotation sequence when the first acceleration measurement is taken.

$T_{Meas}$  = Time interval for making each SRT acceleration measurement at start and end of a rotation sequence.

$t_{SeqStrt}$  = Start time of the first stationary acceleration measurement averaging process for a rotation sequence.

$\underline{u}_{Dwn}^{B_{Strt}}$  = SRT computed downward unit vector (along plumb-bob gravity) in  $B_{Strt}$  frame coordinates.

$\underline{u}_{Dwn}^{B_{Strt}}, \underline{u}_{Dwn}^{B_{End}}$  = Downward unit vectors in the  $B_{Strt}$  and  $B_{End}$  frames used in SRT measurement error models.

$\underline{u}_{Dwn}^{NED}$  = Unit vector downward (along true plumb-bob gravity) in  $NED$  frame coordinates.

$\underline{u}_i^{B_{i,Strt}}$  = Unit vector along axis of rotation  $i$  in a rotation sequence. Defined for the SRT to be along a particular IMU  $B$  frame axis; e.g., for rotation  $i$  around  $B$  frame axis  $x$ ,  $y$ , or  $z$ ,

$$\underline{u}_i^{B_{i,Strt}} = [1 \ 0 \ 0]^T, [0 \ 1 \ 0]^T, \text{ or } [0 \ 0 \ 1]^T.$$

$v_{ij}$  = Orthogonality error between IMU gyro axes  $i$  and  $j$ .

$x_k$  = Sensor error parameter determined from  $\Delta \hat{a}_{jk}^{B_{Strt}}$ .

### 3. IMPROVED SRT ROTATION SEQUENCES

The improved SRT rotation sequences are defined in Table 1, and were designed in [4, Sect. 6] for execution using a two-axis rotation fixture with outer axis horizontal. The Table 1 sequences assume an IMU mounting on the rotation fixture with  $z$  axis (of a right-handed mutually orthogonal  $x$ ,  $y$ ,  $z$  set) aligned with the inner rotation axis and downward when the outer axis rotation angle is zero. The IMU  $x$ ,  $y$  axis mounting is defined to have the  $y$  axis aligned with the outer rotation fixture axis when the inner axis rotation angle is zero.

For the IMU  $x$ ,  $y$ ,  $z$  axis configuration and rotation definitions, the Table 1 rotation sequences separate into five groups, each for measuring particular IMU sensor error characteristics: 1) Sequences 1 – 3 for  $x$ ,  $y$ ,  $z$  gyro scale factor error, 2) Sequences 4 - 5 for  $y$  to  $z$  and  $z$  to  $x$  gyro-to-gyro orthogonality error, 3) Sequence 6 for  $x$  to  $y$  gyro orthogonality error, 4) Sequences 7 – 12 for accelerometer-to-gyro misalignment error ( $x$  accelerometer to  $y$  gyro,  $x$  accelerometer to  $z$  gyro,  $z$  to  $x$ ,  $z$  to  $y$ ,  $y$  to  $z$ , and  $y$  to  $x$ ), and 5) Sequences 13 – 14 for  $x$ ,  $y$  accelerometer bias. Accelerometer  $z$  bias is obtained from the group 4 sequence 7 measurement component not containing accelerometer-to-gyro misalignment.

TABLE 1  
Improved Strapdown Rotation Test Sequences

Sequence Number	Initial IMU Axis Directions		Initial Rotation		Sequential IMU Axis Rotations
	Vertical Down	Along Outer Rotation Axis	Inner Fixture Angles	Outer Fixture Angles	
1	z	y	0	0	+360 y
2	z	x	+90	0	+360 x
3	x	y	0	-90	+360 z
1a	z	y	0	0	-360 y
2a	z	x	+90	0	-360 x
3a	x	y	0	-90	-360 z
4	z	y	0	0	+180 y, +180 z, +180 y, +180 z
5	z	x	+90	0	+180 x, +180 z, +180 x, +180 z
6	x	y	0	-90	+180 y, +90 z, +180 x, +90 z, +180 y, +90 z, +180 x, +90 z
7	y	x	+90	+90	+180 x
8	z	x	+90	0	+180 x
9	x	y	0	-90	+180 z
10	y	x	+90	+90	+180 z
11	z	y	0	0	+180 y
12	x	y	0	-90	+180 y
13	z	y	0	0	+180 z, +180 y
14	z	x	+90	0	+180 z, +180 x

\*Note - Rotation sequences 1a - 3a are not needed when gyros have no scale factor asymmetry.

#### 4. SRT DATA COLLECTION

From [4, Eqs. (3)], the components of  $\hat{\underline{a}}_{SF}^{BStrt}$  in (1) next represent the ‘‘Reference Frame Accelerations’’ in Fig. 1, the reference frame being the  $B$  frame at the start of a rotation sequence (i.e.,  $B_{Strt}$ ). The  $\hat{\underline{a}}_{SF_{Strt}}^{BStrt}$ ,  $\hat{\underline{a}}_{SF_{End}}^{BStrt}$  components in (1) are outputs from the ‘‘Average Acceleration Algorithm’’ block in Fig. 1, calculated as the average of  $\hat{\underline{a}}_{SF}^{BStrt}$  over a designated time period at the start and end of the rotation sequence.

$$\begin{aligned}
 \hat{\underline{a}}_{SF}^{BStrt} &= \hat{\underline{C}}_B^{BStrt} \tilde{\underline{a}}_{SF}^B & \hat{\underline{a}}_{SF_{Strt}}^{BStrt} &\equiv \left( \hat{\underline{a}}_{SF}^{BStrt} \right)_{StrtAvg} \\
 \hat{\underline{a}}_{SF_{End}}^{BStrt} &\equiv \left( \hat{\underline{a}}_{SF}^{BStrt} \right)_{EndAvg} & \Delta \hat{\underline{a}}_H^{BStrt} &= \left( \hat{\underline{a}}_{SF_{End}}^{BStrt} - \hat{\underline{a}}_{SF_{Strt}}^{BStrt} \right)_H \quad (1) \\
 \hat{\underline{u}}_{Dwn}^{BStrt} &= \hat{\underline{C}}_{NED}^{BStrt} \underline{u}_{Dwn}^{NED} & \underline{u}_{Dwn}^{NED} &= [0 \ 0 \ 1]^T \\
 \hat{\underline{a}}_{StrtDown}^{BStrt} &= \hat{\underline{u}}_{Dwn}^{BStrt} \cdot \hat{\underline{a}}_{SF_{Strt}}^{BStrt} + \underline{g} & \hat{\underline{a}}_{EndDown}^{BStrt} &= \hat{\underline{u}}_{Dwn}^{BStrt} \cdot \hat{\underline{a}}_{SF_{End}}^{BStrt} + \underline{g}
 \end{aligned}$$

Each acceleration averaging measurement typically lasts 10 seconds using a simple linear averaging or average-of-averages type algorithm. The  $\hat{C}_{NED}^{BStrt}$  matrix in (1) is the orientation of the IMU  $B$  frame relative to local  $NED$  (north, east, down) coordinates at the start of the rotation sequence, approximately known from the rotation fixture north orientation in the test facility and IMU mounting orientation on the test fixture. The  $\hat{C}_B^{BStrt}$  matrix in (1) is the output of the Fig. 1 “Attitude Computation” block, calculated from [4, Eqs. (4)] as an integration process in (2) next from the start of each rotation sequence. Note in (2) that the  $\hat{C}_B^{BStrt}$  matrix is initialized at identity, thus designating the  $B$  frame at the start of the sequence as the reference frame in Fig. 1 for “Reference Frame Acceleration” measurements. It is also to be noted that  $\hat{\underline{\omega}}_e^{BStrt}$  in (2) was determined in the [1, 2, 3] approaches as part of lengthy inertial alignment operations.

$$\begin{aligned}\hat{C}_B^{BStrt} &= I + \int_{t_{Strt}}^t \hat{C}_B^{BStrt} \dot{\hat{C}}_B^{BStrt} dt & \dot{\hat{C}}_B^{BStrt} &= \hat{C}_B^{BStrt} \left( \hat{\underline{\omega}}^B \times \right) - \left( \hat{\underline{\omega}}_e^{BStrt} \times \right) \hat{C}_B^{BStrt} \\ \hat{\underline{\omega}}_e^{BStrt} &= \hat{C}_{NED}^{BStrt} \underline{\omega}_e^{NED} & \underline{\omega}_e^{NED} &= [\omega_e \cos l \quad 0 \quad -\omega_e \sin l]^T\end{aligned}\quad (2)$$

## 5. DETERMINING IMU SENSOR ERRORS

Approximate error models for (1) – (2) are derived in [5, Sects. 5 & 6], summarized in [4, Eqs. (5) – (7)], and repeated next, defining the  $\Delta \hat{\underline{a}}_H^{BStrt}$ ,  $\hat{\underline{a}}_{Down}^{BStrt}$ ,  $\hat{\underline{a}}_{Down}^{BEnd}$  measurements as a function of individual gyro and accelerometer error parameters for each rotation sequence in the SRT:

$$\begin{aligned}\underline{\phi}_{End}^{BStrt} &\approx \sum_i C_{B_i, Strt}^{BStrt} \left\{ \begin{array}{l} \left[ \kappa_{LinScal} + \kappa_{Asym} \text{Sign}(\dot{\beta}_i) \right] \underline{u}_i^{B_i, Strt} \theta_i \\ + \left[ I \sin \theta_i + (1 - \cos \theta_i) \left( \underline{u}_i^{B_i, Strt} \times \right) \right] \left( \kappa_{Mis} \underline{u}_i^{B_i, Strt} \right) \end{array} \right\} \\ C_{B_{i+1}, Strt}^{B_i, Strt} &= I + \sin \theta_i \left( \underline{u}_i^{B_i, Strt} \times \right) + (1 - \cos \theta_i) \left( \underline{u}_i^{B_i, Strt} \times \right)^2\end{aligned}\quad (3)$$

$$C_{B_1, Strt}^{BStrt} = I \quad \text{Do } i=1 \text{ To } n : C_{B_{i+1}, Strt}^{BStrt} = C_{B_i, Strt}^{BStrt} C_{B_{i+1}, Strt}^{B_i, Strt} \quad C_{B_{End}}^{BStrt} = C_{B_{n+1}, Strt}^{BStrt}$$

$$\begin{aligned}\delta \underline{a}_{SF Strt}^{BStrt} &\approx -g \left( \lambda_{LinScal} + \lambda_{Mis} + \lambda_{Asym} A_{SF Sign}^{BStrt} \right) \underline{u}_{Down}^{BStrt} + \underline{\lambda}_{Bias} \\ \delta \underline{a}_{SF End}^{BEnd} &\approx -g \left( \lambda_{LinScal} + \lambda_{Mis} + \lambda_{Asym} A_{SF Sign}^{BEnd} \right) \underline{u}_{Down}^{BEnd} + \underline{\lambda}_{Bias}\end{aligned}\quad (4)$$

$$\Delta \underline{a}_H^{BStrt} \approx g \underline{u}_{Down}^{BStrt} \times \underline{\phi}_{End}^{BStrt} + \left( C_{B_{End}}^{BStrt} \delta \underline{a}_{SF End}^{BEnd} - \delta \underline{a}_{SF Strt}^{BStrt} \right)_H \quad (5)$$

$$\underline{u}_{Down}^{BEnd} = \left( C_{B_{End}}^{BStrt} \right)^T \underline{u}_{Down}^{BStrt} \quad \underline{a}_{Strt Down}^{BStrt} \approx \underline{u}_{Down}^{BStrt} \cdot \delta \underline{a}_{SF Strt}^{BStrt} \quad \underline{a}_{End Down}^{BEnd} \approx \underline{u}_{Down}^{BEnd} \cdot \delta \underline{a}_{SF End}^{BEnd}$$

Eqs. (3) are derived in [5, Sect. 5.6] as an analytical integration of  $\dot{\phi}^{B Srt}$  (the rate of change of the error in  $\widehat{C}_B^{B Srt}$ ) over a rotation sequence, assuming that each rotation in the sequence is around one of the IMU axes, and which neglects gyro bias and noise effects as negligible for the short time of a rotation sequence. Elements within the (3) - (4) error parameter matrices and vectors are defined in (6) – (7) next.

$$\kappa_{LinScal} = \begin{bmatrix} \kappa_{xx} & 0 & 0 \\ 0 & \kappa_{yy} & 0 \\ 0 & 0 & \kappa_{zz} \end{bmatrix} \quad \kappa_{Mis} = \begin{bmatrix} 0 & \kappa_{xy} & \kappa_{xz} \\ \kappa_{yx} & 0 & \kappa_{yz} \\ \kappa_{zx} & \kappa_{zy} & 0 \end{bmatrix} \quad \kappa_{Asym} = \begin{bmatrix} \kappa_{xxx} & 0 & 0 \\ 0 & \kappa_{yyy} & 0 \\ 0 & 0 & \kappa_{zzz} \end{bmatrix} \quad (6)$$

$$\lambda_{LinScal} = \begin{bmatrix} \lambda_{xx} & 0 & 0 \\ 0 & \lambda_{yy} & 0 \\ 0 & 0 & \lambda_{zz} \end{bmatrix} \quad \lambda_{Mis} = \begin{bmatrix} 0 & \lambda_{xy} & \lambda_{xz} \\ \lambda_{yx} & 0 & \lambda_{yz} \\ \lambda_{zx} & \lambda_{zy} & 0 \end{bmatrix} \quad (7)$$

$$\lambda_{Asym} = \begin{bmatrix} \lambda_{xxx} & 0 & 0 \\ 0 & \lambda_{yyy} & 0 \\ 0 & 0 & \lambda_{zzz} \end{bmatrix} \quad \underline{\lambda}_{Bias} = \begin{bmatrix} \lambda_x \\ \lambda_y \\ \lambda_z \end{bmatrix}$$

Eqs. (6) – (7) for the (3) – (4) sensor error matrices and vectors represent residual errors in the Fig. 1 “Compensation Equations” that have been pre-calibrated prior to the SRT [4, Sect. 4.3.1] for previously known sensor error effects (e.g., thermal sensitivity, non-linearities, or results from a previous SRT). Equating the (1) measurements to the equivalent (5) error model for each rotation sequence provides a simultaneous set of linear equations that are inverted by the SRT to determine the (6) – (7) sensor error parameters.

Gyro misalignments in (6) are relative to an arbitrarily selected coordinate frame  $B$  representing IMU inertial sensor axes. To minimize second order error effects, it is expeditious to select the  $B$  frame to correspond with  $MARS$  (mean angular rate sensor) axes, the orthogonal frame that best fits around the actual gyro input axes. Fig. 2 illustrates the concept.

In Fig. 2,  $\gamma_k$  is the angle between  $MARS$  and general  $B$  frame axes  $i$  and  $j$ . From Fig. 2, defining the  $B$  frame to be a  $MARS$  type is equivalent to setting  $\gamma_k = 0$  for which

$$\kappa_{ij} = \kappa_{ji} \quad (8)$$

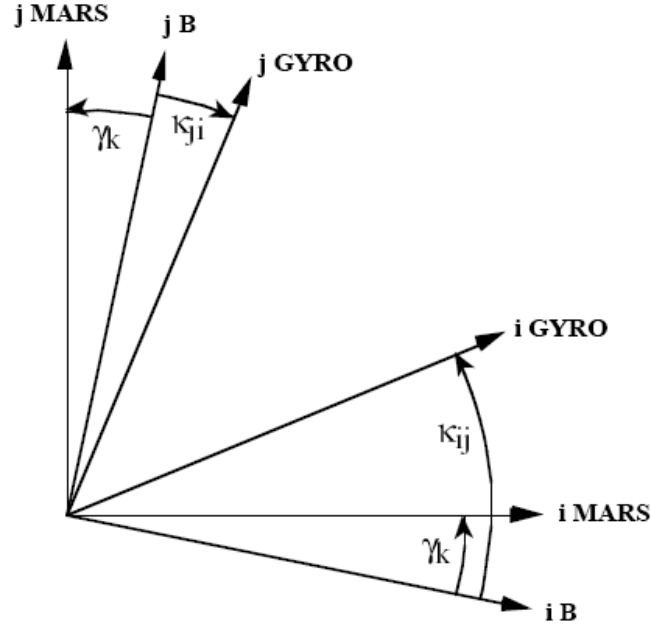


Fig. 2 - *MARS* Coordinates

When adopting a *MARS* frame for *B*, it is also expedient to redefine  $\kappa_{ij}$  in terms of the angular orthogonality error between *i* and *j*, i.e., the angle between *i* and *j* gyro axes compared with the nominal orthogonal *MARS* axes equivalent of  $\pi/2$ . From Fig. 2, the conversion formula is

$$v_{ij} = \kappa_{ij} + \kappa_{ji} \quad (9)$$

or with (8),

$$\kappa_{ij} = \kappa_{ji} = \frac{1}{2} v_{ij} \quad (10)$$

For a *MARS B* frame, the 6 accelerometer  $\lambda_{ij}$  misalignments in (7) will automatically become *MARS* reference specialized. To identify *MARS* specialization and compatibility with *MARS* referenced gyro misalignments in (10), we will utilize the accelerometer misalignment definition formula:

$$\lambda_{ij} = \mu_{ij} \quad (11)$$

## 6. MEASUREMENTS IN TERMS OF SENSOR ERRORS

Eqs. (3) - (5) with (6) - (7) are linearized approximations to the (1) - (2) measurements for each SRT rotation sequence. Section 6 in [4] provides a generic SRT rotation sequence design approach, deriving formulas for generating a particular sensor error signature in a component of the  $\hat{\Delta a}_H^{BStrt}$ ,  $\hat{a}_{StrtDown}^{BStrt}$ , or  $\hat{a}_{EndDown}^{BEnd}$  measurement in (5). Based on the (3) - (7), (10), and (11) analytical model, the [4, Sect. 6] process designed the Table 1 measurements and rotation sequences, producing the following (12) component values for the (5) measurements.

$$\begin{aligned}
\Delta a_{x1}^{BStirt} &= -2\pi g (\kappa_{yy} + \kappa_{yyy}) & \Delta a_{y2}^{BStirt} &= 2\pi g (\kappa_{xx} + \kappa_{xxx}) & \Delta a_{y3}^{BStirt} &= -2\pi g (\kappa_{zz} + \kappa_{zzz}) \\
\Delta a_{x1a}^{BStirt} &= 2\pi g (\kappa_{yy} - \kappa_{yyy}) & \Delta a_{y2a}^{BStirt} &= -2\pi g (\kappa_{xx} - \kappa_{xxx}) & \Delta a_{y3a}^{BStirt} &= 2\pi g (\kappa_{zz} - \kappa_{zzz}) \\
\Delta a_{y4}^{BStirt} &= 4g v_{yz} & \Delta a_{x5}^{BStirt} &= 4g v_{zx} & \Delta a_{y6}^{BStirt} &= 4g v_{xy} & \Delta a_{x7}^{BStirt} &= 2g (\mu_{xy} + v_{xy} / 2) \\
\Delta a_{z7}^{BStirt} &= -2 \left[ \lambda_z + (\pi g / 2) (\kappa_{xx} + \kappa_{xxx}) \right] & a_{Down7}^{BStirt} &= -g (\lambda_{yy} - \lambda_{yyy}) + \lambda_y \\
& & a_{Down7}^{BEnd} &= -g (\lambda_{yy} + \lambda_{yyy}) - \lambda_y & & & & (12) \\
\Delta a_{x8}^{BStirt} &= 2g (\mu_{xz} + v_{zx} / 2) & a_{Down8}^{BStirt} &= -g (\lambda_{zz} - \lambda_{zzz}) + \lambda_z & a_{Down8}^{BEnd} &= -g (\lambda_{zz} + \lambda_{zzz}) - \lambda_z \\
\Delta a_{z9}^{BStirt} &= 2g (\mu_{zx} + v_{zx} / 2) & a_{Down9}^{BStirt} &= -g (\lambda_{xx} - \lambda_{xxx}) - \lambda_x & a_{Down9}^{BEnd} &= -g (\lambda_{xx} + \lambda_{xxx}) + \lambda_x \\
& & \Delta a_{z10}^{BStirt} &= 2g (\mu_{yz} + v_{yz} / 2) & \Delta a_{y11}^{BStirt} &= 2g (\mu_{yz} + v_{yz} / 2) \\
\Delta a_{y12}^{BStirt} &= 2g (\mu_{yx} + v_{xy} / 2) & \Delta a_{y13}^{BStirt} &= -2 (\lambda_y + g v_{yz}) & \Delta a_{x14}^{BStirt} &= -2 (\lambda_x + g v_{zx})
\end{aligned}$$

## 7. SENSOR ERRORS IN TERMS OF MEASUREMENTS

SRT determination of residual errors in the Fig. 1 compensation equations is based on the inverse of (12) with actual (1) measurements substituted for the  $\Delta a_{jk}^{BStirt}$ ,  $a_{Downk}^{BStirt}$ ,  $a_{Downk}^{BEnd}$  error model equivalents. Because the Table 1 rotation sequences have been designed to excite a particular sensor error, the inversion process is trivial, yielding:

$$\begin{aligned}
\kappa_{yy} &= -\frac{1}{4\pi g} (\Delta \hat{a}_{x1}^{BStirt} - \Delta \hat{a}_{x1a}^{BStirt}) & \kappa_{xx} &= \frac{1}{4\pi g} (\Delta \hat{a}_{y2}^{BStirt} - \Delta \hat{a}_{y2a}^{BStirt}) \\
\kappa_{zz} &= -\frac{1}{4\pi g} (\Delta \hat{a}_{y3}^{BStirt} - \Delta \hat{a}_{y3a}^{BStirt}) & \kappa_{yyy} &= -\frac{1}{4\pi g} (\Delta \hat{a}_{x1}^{BStirt} + \Delta \hat{a}_{x1a}^{BStirt}) \\
\kappa_{xxx} &= \frac{1}{4\pi g} (\Delta \hat{a}_{y2}^{BStirt} + \Delta \hat{a}_{y2a}^{BStirt}) & \kappa_{zzz} &= -\frac{1}{4\pi g} (\Delta \hat{a}_{y3}^{BStirt} + \Delta \hat{a}_{y3a}^{BStirt}) \\
v_{yz} &= \frac{1}{4g} \Delta \hat{a}_{y4}^{BStirt} & v_{zx} &= \frac{1}{4g} \Delta \hat{a}_{x5}^{BStirt} & v_{xy} &= \frac{1}{4g} \Delta \hat{a}_{y6}^{BStirt} \\
\lambda_x &= -\frac{1}{2} \Delta \hat{a}_{x14}^{BStirt} - g v_{zx} & \lambda_y &= -\frac{1}{2} \Delta \hat{a}_{y13}^{BStirt} - g v_{yz} \\
\lambda_z &= -\frac{1}{2} \left[ \Delta \hat{a}_{z7}^{BStirt} + \pi g (\kappa_{xx} + \kappa_{xxx}) \right]
\end{aligned} \tag{13}$$

(Continued)

(13) Concluded

$$\begin{aligned}
\mu_{xy} &= \frac{1}{2g} \left( \Delta \hat{a}_{x7}^{BStrt} - g v_{xy} \right) & \mu_{xz} &= \frac{1}{2g} \left( \Delta \hat{a}_{x8}^{BStrt} - g v_{zx} \right) & \mu_{yx} &= \frac{1}{2g} \left( \Delta \hat{a}_{y12}^{BStrt} - g v_{xy} \right) \\
\mu_{yz} &= \frac{1}{2g} \left( \Delta \hat{a}_{y11}^{BStrt} - g v_{yz} \right) & \mu_{zx} &= \frac{1}{2g} \left( \Delta \hat{a}_{z9}^{BStrt} - g v_{zx} \right) & \mu_{zy} &= \frac{1}{2g} \left( \Delta \hat{a}_{z10}^{BStrt} - g v_{yz} \right) \\
\lambda_{yy} &= -\frac{1}{2g} \left( \hat{a}_{Down7}^{BEnd} + \hat{a}_{Down7}^{BStrt} \right) & \lambda_{yyy} &= -\frac{1}{2g} \left( \hat{a}_{Down7}^{BEnd} - \hat{a}_{Down7}^{BStrt} - 2 \lambda_y \right) \\
\lambda_{zz} &= -\frac{1}{2g} \left( \hat{a}_{Down8}^{BEnd} + \hat{a}_{Down8}^{BStrt} \right) & \lambda_{zzz} &= -\frac{1}{2g} \left( \hat{a}_{Down8}^{BEnd} - \hat{a}_{Down8}^{BStrt} - 2 \lambda_z \right) \\
\lambda_{xx} &= -\frac{1}{2g} \left( \hat{a}_{Down9}^{BEnd} + \hat{a}_{Down9}^{BStrt} \right) & \lambda_{xxx} &= -\frac{1}{2g} \left( \hat{a}_{Down9}^{BEnd} - \hat{a}_{Down9}^{BStrt} - 2 \lambda_x \right)
\end{aligned}$$

If the gyros have no asymmetrical scale factor error (i.e.,  $\kappa_{xxx}$ ,  $\kappa_{yyy}$ ,  $\kappa_{zzz} = 0$ ), rotation sequences 1a - 3a would not be used, and the gyro linear scale factor terms in (13) would be computed as in (14).

$$\kappa_{yy} = -\frac{1}{2\pi g} \Delta \hat{a}_{x1}^{BStrt} \quad \kappa_{xx} = \frac{1}{2\pi g} \Delta \hat{a}_{y2}^{BStrt} \quad \kappa_{zz} = -\frac{1}{2\pi g} \Delta \hat{a}_{y3}^{BStrt} \quad (14)$$

Note that accelerometer misalignment ( $\mu_{ij}$ ) and  $x$ ,  $y$  bias ( $\lambda_x$ ,  $\lambda_y$ ) equations in (13) include  $v_{xy}/2$ ,  $v_{yz}/2$ ,  $v_{zx}/2$  gyro-to-gyro orthogonality error offsets. Orthogonality errors are directly available from the rotation sequence 4 - 6 measurements in (12), whence, they can be removed from the  $\mu_{ij}$  and  $\lambda_x$ ,  $\lambda_y$  equations. Similarly, the  $z$  accelerometer bias ( $\lambda_z$ ) in (13) includes a  $\pi g(\kappa_{xx} + \kappa_{xxx})/2$  gyro scale factor error offset that is directly available for (13) removal from  $\Delta \hat{a}_{y2}^{BStrt}$  in (12). Finally, the  $\lambda_{xxx}$ ,  $\lambda_{yyy}$ ,  $\lambda_{zzz}$  accelerometer scale factor asymmetry equations in (13) include  $\lambda_x/2$ ,  $\lambda_y/2$ ,  $\lambda_z/2$  accelerometer bias offsets. After accelerometer biases are computed, they can be removed from the  $\lambda_{xxx}$ ,  $\lambda_{yyy}$ ,  $\lambda_{zzz}$  equations.

## 8. SRT ACCURACY ENHANCEMENT BY ITERATION

The error analysis in Section 9 shows that the SRT is capable of determining sensor compensation errors to a few  $\mu$ rads accuracy (using pre-calibrated sensor scale factors to 1000 ppm accuracy, and 1 milli-rad accuracy in executing rotation sequences, aligning the sensors within the IMU, and aligning the IMU on the rotation fixture). If IMU mounting, rotation execution, and pre-calibration errors are larger,  $\mu$ rad accuracy can still be achieved by repeating the SRT on the IMU using updated sensor calibration coefficients determined from a previous SRT. Modern computer/memory technology make this a trivial operation if SRT computations are structured as a batch-type post-processing operation on IMU sensor data recorded during each Table 1 rotation sequence (e.g., the IMU outputs in Fig. 1). SRT operations would then be

executed by “playing back” the recorded data in “simulated” past time through (1) - (2) and applying (13) to determine the Fig. 1 compensation errors. With this type of structure, the sensor compensation coefficients would be corrected for SRT results from the first play-back, and a second playback executed to determine and correct error residuals remaining in the corrected coefficients. Thus, the iteration would be performed digitally using recorded data from a single execution of the Table 1 rotation sequences.

## 9. SRT ACCURACY ANALYSIS

Sensor compensation error determination with (13) and the Table 1 rotation sequences, is based on linearized approximations in the (3) – (5) generalized SRT measurement model that neglects second order terms (products of errors), rotation fixture imperfections in executing rotations, IMU mounting anomalies on the test fixture (to vertical and relative to north), gyro bias calibration errors, and sensor noise effects. This section analytically evaluates the errors induced by these approximations in determining sensor compensation errors with the improved SRT. Of particular interest is the impact of initial IMU uncertainty relative to north/vertical and errors induced by rotation fixture imperfections, both ultimately affecting production cost.

Analytically assessing the impact of approximations in (3) – (5) and (13) on SRT sensor error determination accuracy is greatly facilitated by having had each of the Table 1 rotation sequences designed to excite a particular error source. As a result, the SRT error model outputs in (12) and their inverse in (13) can be represented by the simple algebraic equations:

$$\Delta a_{jk}^{BStrt} = \pm H_k x_k \quad x_k = \pm \Delta \hat{a}_{jk}^{BStrt} / H_k \quad (15)$$

From (12) and (13), the value of  $H_k$  in (15) for each of the  $x_k$  errors is summarized in Table 2.

From (15) it can be concluded that determination of sensor error parameter  $x_k$  will contain error  $\delta x_k$  due to  $e(\Delta a_{jk}^{BStrt})$  approximation errors in the SRT  $\Delta a_{jk}^{BStrt}$  model:

$$\delta x_k = \pm \frac{1}{H_k} e(\Delta a_{jk}^{BStrt}) \quad (16)$$

Eq. (16) will be the basis in this section for assessing the impact of unmodelled SRT measurement error sources on sensor error parameter determination accuracy.

TABLE 2  
Measurement Sensitivity To Sensor Errors

Error Type	$x_k$	$H_k$
Gyro Scale Factor Error	$(\kappa_{yy} + \kappa_{yyy}), (\kappa_{xx} + \kappa_{xxx}), (\kappa_{zz} + \kappa_{zzz}),$ $(\kappa_{yy} - \kappa_{yyy}), (\kappa_{xx} - \kappa_{xxx}), (\kappa_{zz} - \kappa_{zzz})$	
Gyro-To-Gyro Orthogonality Error	$v_{yz}, v_{zx}, v_{xy}$	$4g$
Accel-To-Gyro Misalignment And Accel Bias Error	$(\mu_{xy} + v_{xy} / 2), (\mu_{xz} + v_{zx} / 2),$ $(\mu_{zx} + v_{zx} / 2), (\mu_{zy} + v_{yz} / 2),$ $(\mu_{yz} + v_{yz} / 2), (\mu_{yx} + v_{xy} / 2),$ $(\lambda_y / g + v_{yz}), (\lambda_x / g + v_{zx}),$ $[\lambda_z / g + (\pi / 2)(\kappa_{xx} + \kappa_{xxx})]$	$2g$

Ref. [4, Eqs. (25) – (27)] shows that SRT measurement model approximation errors in (3) – (5), are the following for each rotation sequence:

$$\begin{aligned}
 e(\underline{\phi}^{BStrt}) &= \int_{t_{Strt}}^t e(\dot{\underline{\phi}}^{BStrt}) dt & e(\underline{\phi}^{BStrt}) &= e(\underline{\phi}^{BStrt}) @ t = t_{End} \\
 e(\dot{\underline{\phi}}^{BStrt}) &= C_B^{BStrt} (\underline{\kappa}_{Bias} + \delta\underline{\omega}_{Quant} + \delta\underline{\omega}_{Rndm}) \\
 + C_B^{BStrt} (\kappa_{LinScal} + \kappa_{Mis} + \kappa_{Asym} \Omega_{EBSign}^B) \underline{\omega}_e^B + (\underline{\phi}^{BStrt} - \underline{\alpha}^{BStrt}) \times \underline{\omega}_e^{BStrt} & (17) \\
 + (\underline{\alpha}^{BStrt} - \underline{\alpha}^{BStrt}) \times \left[ C_B^{BStrt} (\kappa_{LinScal} + \kappa_{Mis} + \kappa_{Asym} \Omega_{EBSign}^B) \underline{\omega}_{EB}^B \right] \\
 + C_B^{BStrt} \left[ (\kappa_{LinScal} + \kappa_{Mis} + \kappa_{Asym} \Omega_{EBSign}^B) (\dot{\underline{\alpha}}^B - \underline{\alpha}^B \times \underline{\omega}_{EB}^B) \right] \\
 e(\delta\underline{a}_{SFStrt}^{BStrt}) &= \underline{\lambda}_{QuantStrt} + \underline{\lambda}_{RndmStrt} + g (\lambda_{LinScal} + \lambda_{Mis} + \lambda_{Asym} A_{SFSign}^{BStrt}) (\underline{\alpha}^{BStrt} \times \underline{u}_{Dwn}^{BStrt}) \\
 e(\delta\underline{a}_{SFEnd}^{BEnd}) &= \underline{\lambda}_{QuantEnd} + \underline{\lambda}_{RndmEnd} + g (\lambda_{LinScal} + \lambda_{Mis} + \lambda_{Asym} A_{SFSign}^{BEnd}) (\underline{\alpha}^{BEnd} \times \underline{u}_{Dwn}^{BEnd}) & (18) \\
 e(\Delta\underline{a}_H^{BStrt}) &= g \underline{u}_{Dwn}^{BStrt} \times \left[ e(\underline{\phi}^{BStrt}) + \left( \frac{1}{2} \underline{\phi}^{BStrt} - \underline{\alpha}^{BStrt} \right) \times \underline{\phi}^{BStrt} \right] \\
 + \left[ C_{BEnd}^{BStrt} e(\delta\underline{a}_{SFEnd}^{BEnd}) - e(\delta\underline{a}_{SFStrt}^{BStrt}) + (\underline{\phi}^{BStrt} + \underline{\alpha}^{BStrt} - \underline{\alpha}^{BStrt}) \times (C_{BEnd}^{BStrt} \delta\underline{a}_{SFEnd}^{BEnd}) \right]_H & (19)
 \end{aligned}$$

Eqs. (17) – (19) contain both first and second order terms, all deemed negligible in [5, Sect. 6] compared to the dominant first order terms in the SRT (3) – (5) error model.

The second order terms comprise products of  $\underline{\alpha}$  (IMU mounting error and rotation fixture inaccuracy) with gyro misalignment and scale factor errors ( $\kappa_{Mis}$ ,  $\kappa_{LinScal}$ ,  $\kappa_{Asym}$ ), and with  $\underline{\phi}^{BStrt}$  angular error in  $\hat{C}_B^{BStrt}$ . (Note: The integral of  $\dot{\underline{\alpha}}^B$  in (17) over a rotation sequence is bounded by natural mechanical constraints, hence, generates the same effect on  $e(\underline{\phi}^{BStrt})$  as  $\underline{\alpha}^B \times \underline{\omega}_{EB}^B$ , the  $\underline{\alpha}^B$  product with IMU angular rate relative to the earth.) For  $\underline{\phi}^{BStrt}$ ,  $\underline{\alpha}$ , and gyro errors on the order of one milli-rad, the effect on  $e(\Delta \underline{a}_H^{BStrt})$  in (19) would be to generate an error on the order of one  $\mu g$ . Based on (16) and Table 2 then, the associated error in SRT sensor error determination would be on the order of one  $\mu rad$ ,  $\mu g$ , or ppm (depending on sensor error type). The Section 8 iteration process would render these error sources negligible.

The first order terms in (17) – (19) consist of integrated gyro random noise ( $\delta \underline{\omega}_{Quant}$ ,  $\delta \underline{\omega}_{Rndm}$ ) into  $e(\underline{\phi}^{BStrt})$ ; accelerometer random noise ( $\underline{\lambda}_{Quant}$ ,  $\underline{\lambda}_{Rndm}$ ) in SRT acceleration measurement error  $e(\Delta \underline{a}_H^{BStrt})$ ; earth rate  $\underline{\omega}_e^{BStrt}$  coupling into  $e(\underline{\phi}^{BStrt})$  from  $\underline{\phi}^{BStrt}$ ,  $\underline{\alpha}_{Strt}^{BStrt}$ , and gyro errors ( $\kappa_{LinScal}$ ,  $\kappa_{Mis}$ ,  $\kappa_{Asym}$ ); and  $\underline{\kappa}_{Bias}$  gyro bias integration into  $e(\underline{\phi}^{BStrt})$ . Importantly, no first order  $\underline{\alpha}_{Strt}^{BStrt}$  terms appear directly in  $e(\Delta \underline{a}_H^{BStrt})$ ; they cancel in (1) for  $\Delta \hat{\underline{a}}_H^{BStrt}$  by the before/after subtraction operation adopted from [3].

## 9.1 GYRO RANDOM NOISE EFFECTS

On a root-mean-square (rms) average basis, integrated  $\delta \underline{\omega}_{Rndm}$  gyro random noise propagates into  $e(\underline{\phi}^{BStrt})$  as the square root of the integration time. For a 40 second rotation sequence time interval and 0.002 deg/ $\sqrt{hr}$  gyro random noise, the rms build-up in  $e(\underline{\phi}_{-End}^{BStrt})$  would be  $[0.002 / (57.3 \times \sqrt{3,600})] \times \sqrt{40} \times 1.E6 = 3.7 \mu rad$ . The effect on  $e(\Delta \underline{a}_H^{BStrt})$  in (19) will be 3.7  $\mu gs$ . From (16) and Table 2, this translates into gyro scale-factor, misalignment errors of 0.59 ppm, 0.93  $\mu rad$ , and accelerometer misalignment, bias errors of 1.8  $\mu rad$ , 1.8  $\mu gs$ .

The integral of  $\delta \underline{\omega}_{Quant}$  gyro quantization noise over a time interval is the rms of the difference between the integrated gyro output pulse quantization error at the start and end of the time interval [2, Sect. 19.2]. For an output pulse size of  $\varepsilon$ , this translates into an rms quantization error of  $\sqrt{(\varepsilon^2 / 12)} \times 2 = 0.41 \varepsilon$ . For a 0.5 arc-sec pulse size, the rms impact on  $e(\underline{\phi}_{-End}^{BStrt})$  would

be on the order of  $0.41 \times [0.5 / (3600 \times 57.3)] \times 1.E6 = 0.99 \mu\text{rad}$ . The rms effect on  $e(\Delta \underline{a}_H^{BStrt})$  in (19) would then be  $0.99 \mu\text{gs}$ . With (16) and  $H_k$  from Table 2, this translates into gyro scale-factor, misalignment errors of 0.16 ppm,  $0.25 \mu\text{rad}$ , and accelerometer misalignment, bias errors of  $0.50 \mu\text{rad}$ ,  $0.50 \mu\text{gs}$ .

## 9.2 ACCELEROMETER RANDOM NOISE EFFECTS

The impact of accelerometer output noise on SRT accuracy can be assessed by analyzing how  $\underline{\lambda}_{Quant}$  and  $\underline{\lambda}_{Rndm}$  impact  $e(\delta \hat{\underline{a}}_{SF Strt}^{BStrt})$  and  $e(\delta \hat{\underline{a}}_{SF End}^{BEnd})$  in (18), hence,  $e(\Delta \underline{a}_H^{BStrt})$  in (19). The start and end effects can be analyzed separately, each using an approach similar to that taken for the  $\delta \underline{\omega}_{Rndm}$  and  $\delta \underline{\omega}_{Quant}$  analysis. The difference is that the integration time interval would be the averaging times to measure  $\hat{\underline{a}}_{SF Strt}^{BStrt}$  and  $\hat{\underline{a}}_{SF End}^{BStrt}$  in (1). Propagation of  $\underline{\lambda}_{Rndm Strt}$  and  $\underline{\lambda}_{Rndm End}$  over the start and end averaging times is unaffected by the averaging algorithm, generating the same rms error as a simple integration process (i.e., proportional to the square-root of the integration times). Some averaging algorithms are designed to reduce the impact of  $\underline{\lambda}_{Quant}$  noise from what would be generated using a direct linear averaging process, e.g., an average-of-averages type algorithm [3, Sect. 18.4.7.3].

## 9.3 EARTH RATE COUPLING EFFECTS

An important new advantage for the improved SRT is elimination of the requirement for inertial self-alignment of the IMU prior to rotation sequence execution, a problem area for IMUs with lesser accuracy gyros. This requires a reasonably accurate initial physical alignment of the IMU on the test fixture relative to north (e.g., 1 milli-rad). The  $\underline{\alpha}_{Strt}^{BStrt} \times \underline{\omega}_e^{BStrt}$  term in (17) becomes the  $e(\dot{\underline{\phi}}^{BStrt})$  error introduced with this approach, dependent on the total time over a rotation sequence for the error to integrate into  $e(\underline{\phi}_{End}^{BStrt})$ . Assuming 10 seconds each for acceleration measurements (before and after rotation sequence execution) and 20 seconds for rotations, the total time for a sequence will be 40 seconds. Then the integral of  $\underline{\alpha}_{Strt}^{BStrt} \times \underline{\omega}_e^{BStrt}$  over the rotation sequence will be  $\alpha \times \text{earth rate} \times 40$ . For  $\alpha$  of 1 milli-rad and earth rate = 15 deg/hr (0.000073 rad/sec), this translates into an  $e(\underline{\phi}_{End}^{BStrt})$  value of  $0.001 \times 0.000073 \times 40 \times 1.E6 = 2.9 \mu\text{rad}$ , thereby impacting  $e(\Delta \hat{\underline{a}}^{BStrt})$  in (19) by  $2.9 \mu\text{g}$ . With (16) and  $H_k$  from Table 2, this translates into gyro scale-factor, misalignment errors of 0.46 ppm,  $0.73 \mu\text{rad}$ , and accelerometer misalignment, bias errors of  $1.5 \mu\text{rad}$ ,  $1.5 \mu\text{gs}$ .

A similar analysis would show that for  $\kappa_{LinScal}$ ,  $\kappa_{Mis}$ ,  $\kappa_{Asym}$ , and  $\underline{\phi}^{B_{Strt}}$  on the order of one milli-rad, their products with earth rate in (17) would also generate components in  $e\left(\underline{\phi}_{End}^{B_{Strt}}\right)$  on the order of 0.46 to 1.5  $\mu\text{rad}$ . However, if the SRT is iterated once (as described in Section 8) using sensor compensation in Fig. 1 that has been corrected for initial SRT results, these error terms would be considerably reduced, making their impact on  $e\left(\underline{\phi}_{End}^{B_{Strt}}\right)$  negligible.

#### 9.4 GYRO BIAS EFFECTS

Because of its importance in SRT applications for lesser accuracy IMUs, the impact of gyro bias on SRT accuracy is analyzed in more detail in [5, Sect. 8] as an analytical integration of  $\underline{\kappa}_{Bias}$  in (17) on  $e\left(\underline{\phi}_{End}^{B_{Strt}}\right)$ . The overall result is shown next in (20) - (21). An analysis of (20) - (21) in [5, Sect. 5.2.6] using (16) for  $\delta x_k$  finds that resulting SRT sensor determination errors for the Table 1 sequences would then be as shown in (22) next.

$$e\left(\underline{\phi}_{End}^{B_{Strt}}\right)_{GyroBias_{Rot}} = \sum_i C_{Bi,Strt}^{B_{Strt}} \left[ I + \frac{(1 - \cos \theta_i)}{\theta_i} \left( \underline{u}_i^{Bi,Strt} \times \right) + \left( 1 - \frac{\sin \theta_i}{\theta_i} \right) \left( \underline{u}_i^{Bi,Strt} \times \right)^2 \right] \frac{\theta_i}{\dot{\beta}_i} \underline{\kappa}_{Bias} \quad (20)$$

$$e\left(\Delta \hat{\underline{a}}_{-H}^{B_{Strt}}\right)_{GyroBias} = g \underline{u}_{Dwn}^{B_{Strt}} \times \left\{ \left( \underline{\phi}_{End}^{B_{Strt}} \right)_{GyroBias_{Rot}} + T_{Meas} \left[ I + F_{Meas} \left( C_{B_{End}}^{B_{Strt}} - I \right) \right] \underline{\kappa}_{Bias} \right\} \quad (21)$$

$$\begin{aligned} e(\kappa_{zz} - \kappa_{zzz})_{GyroBias} &= - \left[ 1 / \dot{\beta} + T_{Meas} / (2\pi) \right] \kappa_z \quad \text{Similarly For Sequences 1, 2, and 1a - 3a} \\ e(v_{zx})_{GyroBias} &= (\kappa_x + \kappa_z) / \dot{\beta} - T_{Meas} \kappa_y / 4 \quad \text{Similarly For Sequence 4} \\ e(v_{xy})_{GyroBias} &= (\kappa_x + \kappa_y) / \dot{\beta} - T_{Meas} \kappa_z / 4 \\ e(\mu_{xy} + v_{xy}/2)_{GyroBias} &= \kappa_y / \dot{\beta} + T_{Meas} (1 - 2 F_{Meas}) \kappa_z / 2 \quad \text{Similarly For Sequences 8 - 12} \\ e[\lambda_z + (\pi g/2)(\kappa_{xx} + \kappa_{xxx})]_{GyroBias} &= -(\pi g/2) \left( 1 / \dot{\beta} + T_{Meas} / \pi \right) \kappa_x \\ e(\lambda_y + g v_{yz})_{GyroBias} &= -g \left[ (\kappa_z + \kappa_y) / \dot{\beta} - T_{Meas} \kappa_x / 2 \right] \quad \text{Similarly For Sequence 14} \end{aligned} \quad (22)$$

Ref. [5, Sect. 8.4] shows that  $F_{Meas}$  in (22) is 1/2, both for a simple linear averaging algorithm and an average-of-averages algorithm. Using  $F_{Meas} = 1/2$ ,  $g = 32.2 \text{ ft/sec}^2$ , and representative values of  $\dot{\beta} = 1 \text{ rad/sec}$  and  $T_{Meas} = 10 \text{ sec}$ , (22) enables evaluation of the effect of neglecting  $\kappa_x$ ,  $\kappa_y$ ,  $\kappa_z$  gyro bias calibration errors. For example, for  $\kappa_x + \kappa_y = 0.1 \text{ deg/hr} = 4.85\text{e-}7 \text{ rad/sec}$  and  $\kappa_z = -0.1 \text{ deg/hr} = -4.85\text{e-}7 \text{ rad/sec}$ , the error in gyro non-orthogonality determination  $e(v_{xy})_{GyroBias}$  in (22) would be 1.7  $\mu\text{rads}$ . As another example, for  $\kappa_y$  gyro bias

of  $4.85e-7$  rad/sec, (22) shows that  $0.49 \mu\text{rad}$  of accelerometer misalignment determination error would be generated in  $e(\mu_{xy} + v_{xy}/2)_{GyroBias}$ . Finally, for  $\kappa_x = 4.85e-7$  rad/sec and  $\kappa_z + \kappa_y = -4.85e-7$  rad/sec, (22) shows that the error in accelerometer bias determination  $e(\lambda_y + g v_{yz})_{GyroBias}$  would be  $9.37e-5 \text{ ft/sec}^2 = 2.91 \mu\text{gs}$ .

Larger than  $0.1 \text{ deg/hr}$  gyro bias calibration errors may require the [4, Sect. 4.8] mitigation process for reduction. For gyros without g-sensitivity, this entails measuring average gyro outputs during the measurement period preceding a rotation sequence, then subtracting the appropriate earth rate component for the rotation sequence starting attitude. For gyros with g-sensitivity, the process requires additional gyro bias measurements at two other IMU orientations.

## 10. CALIBRATING IMU ATTITUDE OUTPUTS

Calibrating an IMU for SRT measured sensor errors corrects IMU computed inertial navigation velocity/position but not attitude outputs [2, Sect. 13.2.4]. Attitude output errors are caused by three misalignments of the IMU sensor assembly relative to the IMU mount in the user vehicle. Ref. [4, Sect. 4.9] describes how IMU-to-mount misalignments are easily measured once the IMU has been calibrated for SRT results. The general method is to install a standard IMU mount on a single axis rotation fixture with the mount shimmed to level, and having its lateral axis (e.g.,  $y$ ) reference flat perpendicular to the fixture horizontal rotation axis. When an IMU is positioned on the mount, the average horizontal compensated accelerometer outputs (e.g.,  $x$  and  $y$ ) would nominally be zero. Non-zero values measure the two misalignments between the sensor-assembly  $x, y$  and the vertical mount  $z$  axis. Pitching the IMU 90 degrees around  $y$  rotates the  $x$  axis to vertical, enabling the  $y$  accelerometer to then measure the third misalignment between the sensor assembly  $y$  axis and the mount  $x$  axis. This process could also be integrated within the SRT during a Section 8 iteration operation.

## REFERENCES

- [1] Savage, P. G., "Calibration Procedures For Laser Gyro Strapdown Inertial Navigation Systems", 9th Annual Electro-Optics / Laser Conference and Exhibition, Anaheim, California, Oct 25-27, 1977.
- [2] Savage, P. G., *Strapdown Analytics*, Strapdown Associates, Inc., Maple Plain, Minnesota, 2000 and Second Edition in 2007.
- [3] Downs, H. B., "A Lab Test To Find The Major Error Sources In A Laser Strapdown Inertial Navigator", 38th Annual Meeting of the ION, Colorado Springs, CO, June 15-17, 1982.
- [4] Savage, P.G., "Improved Strapdown Inertial System Calibration Procedures, Part 1, Procedures, Rotation Fixtures, And Accuracy Analysis", WBN-14020-1, Strapdown Associates, Inc., Jan 11, 2018, free access at [www.strapdownassociates.com](http://www.strapdownassociates.com).

- [5] Savage, P.G., “Improved Strapdown Inertial System Calibration Procedures, Part 2, Analytical Derivations”, WBN-14020-2, Strapdown Associates, Inc., Jan 11, 2018, free access at [www.strapdownassociates.com](http://www.strapdownassociates.com).
- [6] Savage, P.G., “Improved Strapdown Inertial System Calibration Procedures, Part 3, Numerical Examples”, WBN-14020-3, Strapdown Associates, Inc., Jan 11, 2018, free access at [www.strapdownassociates.com](http://www.strapdownassociates.com).